ACCOUNTS
of chemical research

Dioxygen Activation in Soluble Methane Monooxygenase

CHRISTINE E. TINBERG AND STEPHEN J. LIPPARD*

Department of Chemistry, Massachusetts Institute of Technology, Cambridge, Massachusetts 02139, United States

RECEIVED ON NOVEMBER 17, 2010

CONSPECTUS

The controlled oxidation of methane to methanol is a chemical transformation of great value, particularly in the pursuit of alternative fuels, but the reaction remains underutilized industrially because of inefficient and costly synthetic procedures. In contrast, methane monooxygenase enzymes (MMOs) from methanotrophic bacteria achieve this chemistry efficiently under ambient conditions. In this Account, we discuss the first observable step in the oxidation of methane at the carboxylate-bridged diiron active site of the soluble MMO (sMMO), namely, the reductive activation of atmospheric O_2. The results provide benchmarks against which the dioxygen activation mechanisms of other bacterial multicomponent monooxygenases can be measured.

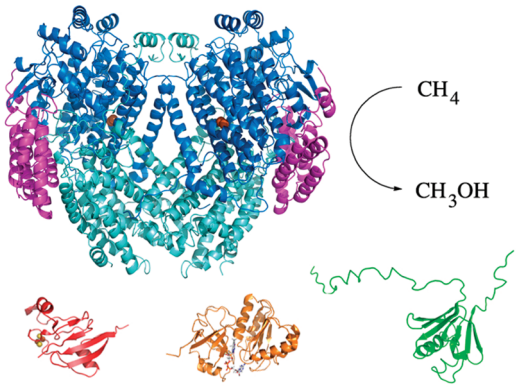

Molecular oxygen reacts rapidly with the reduced diiron(II) center of the hydroxylase component of sMMO (MMOH). The first spectroscopically characterized intermediate that results from this process is a peroxodiiron(III) species, P*, in which the iron atoms have identical environments. P* converts to a second peroxodiiron(III) unit, H_{peroxo}, in a process accompanied by the transfer of a proton, probably with the assistance of a residue near the active site. Proton-promoted O−O bond scission and rearrangement of the diiron core then leads to a diiron(IV) unit, termed Q, that is directly responsible for the oxidation of methane to methanol. In one section of this Account, we provide a detailed discussion of these processes, with particular emphasis on possible structures of the intermediates. The geometries of P* and H_{peroxo} are currently unknown, and recent synthetic modeling chemistry has highlighted the need for further structural characterization of Q, currently assigned as a di(μ-oxo)diiron(IV) "diamond core."

In another section of the Account, we discuss in detail proton transfer during the O_2 activation events. The role of protons in promoting O−O bond cleavage, thereby initiating the conversion of H_{peroxo} to Q, was previously a controversial topic. Recent studies of the mechanism, covering a range of pH values and in D_2O instead of H_2O, confirmed conclusively that the transfer of protons, possibly at or near the active site, is necessary for both P*-to-H_{peroxo} and H_{peroxo}-to-Q conversions. Specific mechanistic insights into these processes are provided.

In the final section of the Account, we present our view of experiments that need to be done to further define crucial aspects of sMMO chemistry. Here our goal is to detail the challenges that we and others face in this research, particularly with respect to some long-standing questions about the system, as well as approaches that might be used to solve them.

Introduction

A current challenge in renewable energy is the development of processes that allow us to generate alternative fuels in a sustainable manner. Methane gas is an abundant precursor of liquid fuels, but current strategies for its selective conversion to methanol, a necessary step in its utilization, are neither economical nor sustainable.[1] Methanotrophic bacteria utilize methane as a sole carbon source. The first step in the metabolism of methane by these organisms is its selective conversion to methanol by methane monooxygenase enzymes (MMOs) (eq 1). Two methane monooxygenases have evolved to

$$CH_4 + O_2 + NADH + H^+ \xrightarrow{MMO} CH_3OH + H_2O + NAD^+ \quad (1)$$

perform this reaction: a membrane-bound particulate MMO (pMMO) present in most methanotrophs and a

Published on the Web 03/10/2011 www.pubs.acs.org/accounts
10.1021/ar1001473

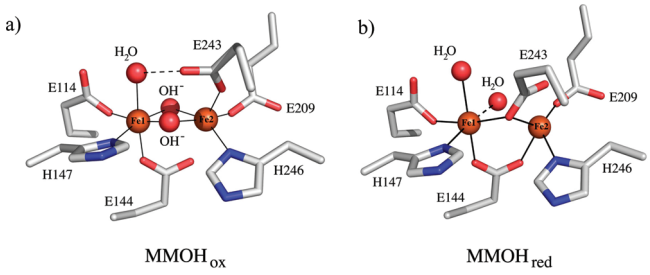

FIGURE 1. Diiron active site structures of (a) *Mc* $MMOH_{ox}$ (PDB ID 1MTY) and (b) *Mc* $MMOH_{red}$ (PDB ID 1FYZ).

soluble MMO (sMMO) expressed in several methanotrophs under copper-limited conditions. Both MMOs utilize a metal center to activate atmospheric dioxygen for attack on the strong C−H bond (104 kcal/mol) of methane. Although the active site of pMMO is probably a dinuclear copper center,[2] that of sMMO is a carboxylate-bridged diiron unit.[3,4] The oxidative chemistry performed at these sites, particularly the latter, has been investigated extensively, elevating our understanding of how Nature utilizes biological methane as an energy source and guiding the development of industrially relevant small molecule catalysts.[5] In this Account, we review recent progress toward understanding biological methane oxidation at the diiron center of sMMO. A groundbreaking study of pMMO is available in the recent literature.[2]

Soluble Methane Monooxygenase

sMMO has been studied primarily in two methanotrophs, *Methylococcus capsulatus* (Bath), hereafter referred to as *Mc*, and *Methylosinus trichosporium* OB3b, hereafter *Mt*. Methane oxidation occurs at a carboxylate-bridged diiron center housed within a hydroxylase protein (MMOH) featuring an $(\alpha\beta\gamma)_2$ dimer architecture.[6] The catalytic active site resides in a four-helix bundle of the α-subunit. The diiron center is coordinated by two histidine and four glutamate ligands (Figure 1). Solvent-derived molecules complete the pseudo-octahedral coordination spheres. In the diiron(III) resting state of the enzyme ($MMOH_{ox}$), two hydroxide ligands bridge the iron atoms, which are separated by ∼3.1 Å (Figure 1a).[6] Upon reduction to the diiron(II) form ($MMOH_{red}$), the bridging solvent molecules depart and E243, which is bound only to Fe1 in $MMOH_{ox}$, assumes a bridging position while remaining chelated to Fe2 (Figure 1b). As a consequence, an open coordination site becomes available and the Fe−Fe distance increases.[7]

The structural features of $MMOH_{ox}$ and $MMOH_{red}$ have been investigated by EXAFS, EPR, ENDOR/ESEEM, MCD, and

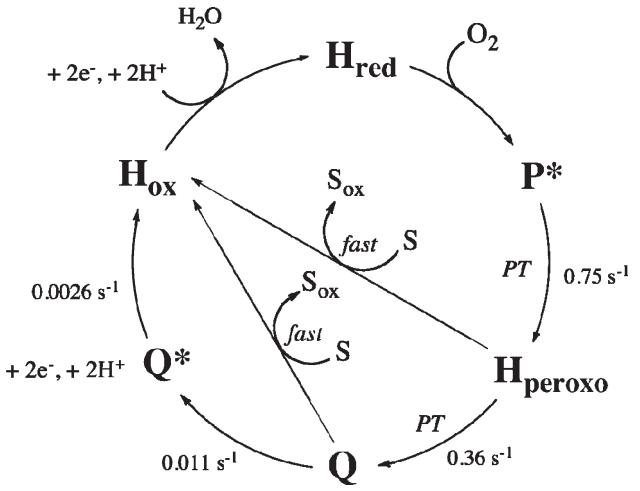

FIGURE 2. *Mc* MMOH catalytic cycle. Rate constants were measured at pH 7.0 and 4 °C. S denotes substrate.

Mössbauer spectroscopy.[3,4] The high-spin Fe(III) ions of $MMOH_{ox}$ are antiferromagnetically coupled, resulting in a diamagnetic ground state. Two hydroxide bridges mediate the spin-exchange. In contrast, the high-spin Fe(II) atoms of $MMOH_{red}$ are weakly ferromagnetically coupled, and the resulting $S = 4$ spin system has a low-energy non-Kramer's doublet that is split in zero applied field, giving rise to a characteristic EPR signal at $g = 16$.

The Reaction of $MMOH_{red}$ with O_2

The reductive activation of O_2 at the diiron(II) center of $MMOH_{red}$ is the first step of the sMMO catalytic cycle (Figure 2). Despite the observation that the diiron active site is buried within the MMOH hydrophobic protein environment, O_2 can access it in a facile manner. The route of O_2 delivery to the active site has been suggested by structural studies. Crystallographic investigations of MMOH revealed several adjacent hydrophobic cavities in the α-subunit that delineate a pathway from the exterior of the protein to the diiron site (Figure 3).[6] Crystals of MMOH pressurized with xenon gas, an electron-rich O_2 and CH_4 surrogate, contained ordered Xe atoms residing almost exclusively in these cavities, suggesting a route by which these substrates might access the active site.[8] An alternative method of substrate ingress, product egress, or both is through a pore formed between two of the helices that provide ligands to the diiron center (Figure 3). Hydrophilic residues line the pore, which has been proposed as a pathway of H_3O^+ translocation.[9]

Upon reaching the diiron(II) center, O_2 rapidly reacts in the presence of 2 equiv of the regulatory protein MMOB.[10,11] The rate constant for O_2-promoted $MMOH_{red}$ decay was

measured to be ~24 s^{-1} at pH 7.0 and 4 °C by rapid freeze-quench (RFQ) Mössbauer spectroscopy in *Mc* MMOH[11] and ~22 s^{-1} at pH 7.7 and 4 °C by RFQ EPR spectroscopy in *Mt* sMMO.[10] For *Mt* $MMOH_{red}$, this process is independent of pH and O_2 concentration between 0.3 and 0.7 mM. One interpretation of these results is that a rapid, irreversible O_2 binding event precedes oxidation of the diiron center.[10] Alternatively, O_2 binding might involve a reversible pre-equilibrium followed by an irreversible chemical reaction with the Michealis constant (K_M) being much lower than the concentrations of O_2 used in the EPR experiments such that the system is saturated.[12] An attempt to find evidence for such a Michaelis complex in *Mc* MMOH using an oxygen electrode failed to detect a tight enzyme–dioxygen interaction, however.[12] It is possible that an irreversible conformational change precedes reaction of O_2 at the diiron center.[13]

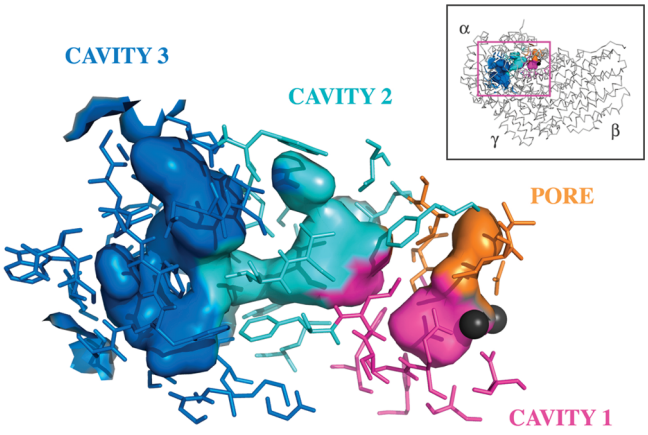

FIGURE 3. Proposed pathways of substrate ingress in MMOH. Three hydrophobic cavities link the diiron center to the protein exterior. A small pore lined by hydrophilic residues also leads to the protein surface. Iron atoms are depicted as gray spheres. PDB 1MTY.

Peroxodiiron(III) Intermediates of MMOH

Computational studies suggest that the first intermediate resulting from reaction of $MMOH_{red}$ with O_2 is a mixed-valent diiron(II/III) superoxide species.[14,15] An oxygen KIE study of CH_3CN oxidation by sMMO returned a value of 1.016, consistent with one-electron reduction of O_2 to superoxide being the first irreversible step in the reaction pathway, although other possibilities could not be definitively ruled out.[12] An Fe(II)/Fe(III) superoxide unit has never been directly observed in a diiron enzyme in which the O_2-activating species is diiron(II), however, most likely because of its transient existence.[16,17]

The first spectroscopically observed intermediate in the reaction of $MMOH_{red}$ with O_2 is a peroxodiiron(III) species. Early kinetic evidence for this unit was provided by studies of the *Mt* system, because the rate constant for O_2-promoted $MMOH_{red}$ decay was significantly faster than that describing formation of the earliest observed oxygenated-iron species arising from the reaction, intermediate Q (vide infra).[10] These observations indicated the presence of at least one additional intermediate preceding Q formation. Direct spectroscopic evidence for such a transient came from studies of *Mc* MMOH.[11,18] The 4.2 K Mössbauer spectrum of this intermediate, termed H_{peroxo},[19] revealed a diamagnetic center having similar iron(III) sites.[18,20] Stopped-flow UV–vis analyses revealed a rich optical profile having distinct features at 420 and 720 nm (Table 1).[21] RFQ Mössbauer and stopped-flow optical spectroscopic studies yielded the same decay rate constant for this intermediate (~0.36 s^{-1} at 4 °C); however, the kinetic parameter describing its formation was found to be different by the two techniques. RFQ Mössbauer experiments returned a rate constant of ~25 s^{-1} at 4 °C, a value in agreement with that measured for $MMOH_{red}$ decay (vide supra).[11] In contrast, stopped-flow studies indicated a value of ~1 s^{-1} at 4 °C.[21,22] Two distinct

TABLE 1. Spectroscopic Parameters of Peroxodiiron(III) Intermediates of Enzymes and Model Complexes

	optical		Mössbauer		peroxide binding mode
	λ_{max} (nm)	ε (M^{-1} cm^{-1})	δ (mm/s)	ΔE_Q (mm/s)	
MMOH H_{peroxo} (*Mc*)	420; 720	3880; 1350[a]	0.66	1.51[b]	
MMOH H_{peroxo} (*Mt*)	725	2500[c]	0.67	1.51[d]	
RNR-R2 D84E	700	1500[e]	0.63	1.58[e]	μ-1,2[f]
Δ^9-desaturase	700	1200[g]	0.68; 0.64	1.90; 1.06[g]	μ-1,2[h]
frog M ferritin	650[i]		0.62	1.08[i]	μ-1,2[j]
hDOHH[k]	630	2800	0.55; 0.58	1.16; 0.88	μ-1,2
$[Fe_2(\mu\text{-}1,2\text{-}O_2)(\mu\text{-}O_2CCH_2Ph)_2\{HB(pz')_3\}_2]^{l}$	694	2650	0.66	1.40	gauche μ-1,2
$[Fe_2(\mu\text{–}OH)(\mu\text{-}1,2\text{-}O_2)(6\text{-}Me_2\text{-}BPP)_2]^{+m}$	644	3000	0.50	1.31	*cis*-μ-1,2
$[Fe_2(\mu\text{-}O)(\mu\text{-}1,2\text{-}O_2)(6\text{-}Me_3\text{-}TPA)_2]^{2+n}$	494; 648	1100; 1200	0.54	1.68	*cis*-μ-1,2

[a]Reference 24. [b]Reference 11. [c]Reference 47. [d]Reference 20. [e]Reference 50. [f]Reference 25. These studies were performed on the D84E/W48F variant. [g]Reference 51. [h]Reference 28. [i]Reference 52. [j]Reference 27. [k]Reference 29. [l]Reference 33. pz′ = 3,5-bis(isopropyl)-pyrazolyl. [m]Reference 53. BPP = *N*,*N*-bis(2-pyridylmethyl)-3-aminopropionate. [n]Reference 54. TPA = tris(2-pyridylmethyl)amine.

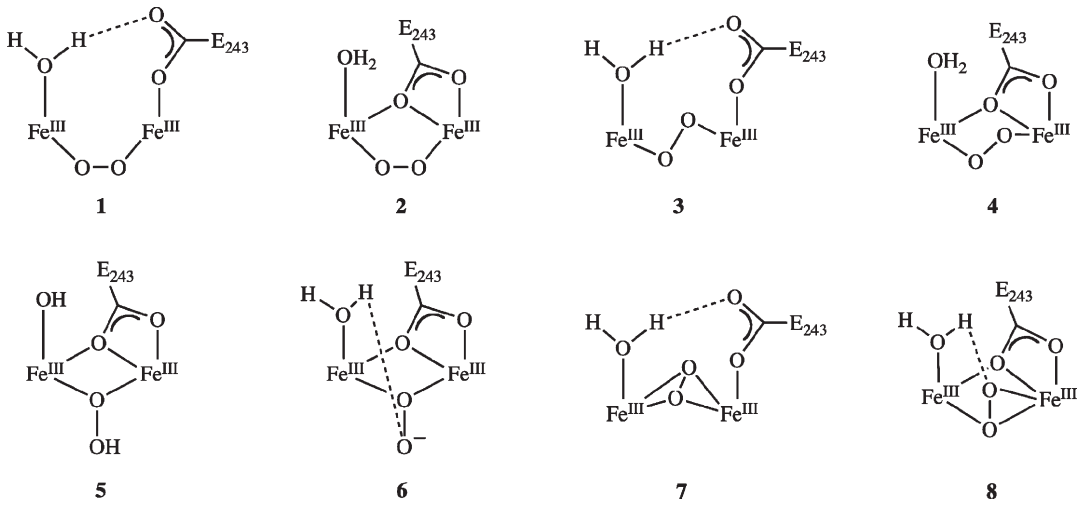

FIGURE 4. Possible structures for the peroxodiiron(III) species of MMOH.

peroxodiiron(III) species having similar Mössbauer parameters but distinct optical signatures were proposed to explain the discrepancy.[21]

Evidence for two peroxodiiron(III) intermediates was provided by stopped-flow optical studies of the *Mt* enzyme.[23] Fits of data monitoring the reaction of $MMOH_{red}$ with O_2 in the presence of MMOB at 430 nm required an additional phase preceding H_{peroxo} formation. The species assigned to this phase, P*, formed with a rate constant of $\sim$22 s^{-1} at 4 °C, consistent with it being the first intermediate resulting from decay of $MMOH_{red}$. From the amplitudes of the kinetic phases revealed by these studies, H_{peroxo}, with k_{form} = 9−12 s^{-1} at 4 °C and pH 7.0, was suggested to have negligible absorbance at 430 nm, an observation inconsistent with that for *Mc* MMOH (vide supra). The authors explained this contradiction by proposing that the signal detected at 420 nm for *Mc* H_{peroxo} was an artifact of the dominant optical contribution of Q at this wavelength.[23] We recently obtained direct optical spectroscopic evidence for P* in *Mc* MMOH,[24] which shows distinct features at 720 nm ($\varepsilon \approx$ 1250 M^{-1} cm^{-1}) and 420 nm ($\varepsilon \approx$ 3500 M^{-1} cm^{-1}). The latter was clearly revealed when reactions were performed in the presence of high concentrations on CH_4 to eliminate the optical contribution of Q at this wavelength. These studies provide conclusive evidence that H_{peroxo} does indeed absorb at 420 nm. This conclusion is important for comparing the properties of H_{peroxo} to those of synthetic peroxodiiron(III) complexes and computational models for the intermediate.

From the similarities in its Mössbauer parameters (vide supra) and optical properties to those of H_{peroxo}, we proposed that P* features an identical Fe_2O_2 core but differs instead in the conformation of the supporting ligands. The exact structures of the sMMOH peroxodiiron(III) species remain a major unsolved question in the field, however. Several possible architectures differing in the geometry of the $\{Fe_2O_2\}^{4+}$ unit as well as the coordination mode of E243 are depicted in Figure 4.

Structural insights can be gleaned from comparing the spectroscopic parameters of P* and H_{peroxo} to those of peroxodiiron(III) intermediates in similar diiron enzymes (Table 1). Peroxide units formed in several of these proteins, including the R2 subunit of ribonucleotide reductase (RNR-R2), have been structurally characterized by resonance Raman (RR) spectroscopy, which indicates a μ-1,2 peroxide binding mode (**1**−**4**) in all cases.[25−29] A *cis*-μ-1,2-peroxide coordination geometry (**1** or **2**) was also suggested from the X-ray crystal structure of the toluene 4-monooxygenase hydroxylase-regulatory protein complex soaked with H_2O_2.[30,31] X-ray crystal structures of several peroxodiiron(III) model compounds are available (Table 1).[5,32] One in particular has Mössbauer parameters that are nearly identical to those of P*, $[Fe_2(\mu\text{-}1,2\text{-}O_2)(\mu\text{-}O_2CCH_2Ph)_2\{HB(pz')_3\}_2]$, where pz′ is 3,5-bis(isopropyl)-pyrazolyl. The crystal structure of this complex reveals a gauche μ-1,2 peroxide configuration (**3** or **4**) (Table 1).[33] High-level theoretical calculations also favor a gauche μ-1,2-peroxo structure for H_{peroxo}.[34] Although a nonplanar μ-η^2:η^2 geometry (**7**) has also been suggested,[14,15,35] it is no longer favored computationally.[36]

Intermediate Q

H_{peroxo} can oxidize electron-rich substrates.[21,37,38] In the absence of such substrates, cleavage of the O−O bond results in its rapid conversion to intermediate Q, an

TABLE 2. Spectroscopic Parameters of Intermediate Q and High-Valent Model Complexes

	optical		Mössbauer		
	λ_{max} (nm)	ε (M^{-1} cm^{-1})	δ (mm/s)	ΔE_Q (mm/s)	Fe−Fe (Å)
MMOH Q (*Mc*)	420	8415[a]	0.21; 0.14	0.68; 0.55[b]	
MMOH Q (*Mt*)	330; 430	7500; 7500[c]	0.17	0.53[d]	2.46[e]
$[Fe_2(\mu\text{-}O)_2(L)_2]^{3+}$	366; 616	7900; 5200[f]	0.48; 0.08	1.6; 0.5[g]	2.683[h]
$[Fe_2(\mu\text{-}O)_2(L)_2]^{4+i}$	485; 875	9800; 2200	−0.04	2.09	2.73

[a]Reference 24. [b]Reference 11. [c]Reference 10. [d]Reference 39. [e]Reference 20. [f]Reference 55. L = 5-Me_3-TPA; TPA = tris(2-pyridylmethyl)amine. [g]Reference 56. L = 6-Me_3-TPA. [h]Reference 57. L = 5-Et_3-TPA. [i]Reference 40. L = tris((4-methoxy-3,5-dimethylpyrid-2-yl)d_2-methyl)amine.

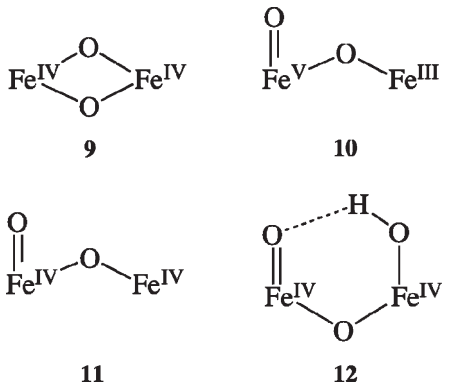

FIGURE 5. Possible structures for the $\{Fe_2O_2\}^{4+}$ core of Q.

antiferromagnetically coupled diiron(IV) unit with absorption bands at ∼350 and ∼420 nm (Table 2).[10,11,18,39] The rate constants for this process are 0.36 and 2.5 s^{-1}, respectively, for the *Mc*[24] and *Mt*[23] enzymes at 4 °C and pH 7.0. The single quadrupole doublet observed in the Mössbauer spectrum of *Mt* Q suggested similar ligand environments for both Fe(IV) atoms (Table 2).[39] In contrast, two equal-intensity quadrupole doublets were detected for *Mc* Q.[11,18] An EXAFS spectrum of *Mt* Q was interpreted in terms of a di(μ-oxo) diiron(IV) "diamond core" structure with a short Fe−Fe distance of 2.46 Å and Fe−O bond lengths of 1.77 and 2.05 Å at each iron atom (Figure 5, **9**).[20] Recent quantum mechanics/molecular mechanics (QM/MM) studies suggest that the short Fe−Fe distance of Q might reflect protein-based compression along the Fe−Fe vector, which provides the necessary driving force to generate the intermediate.[15] On the basis of the EXAFS parameters, the authors proposed a head-to-tail dimer of Fe^{IV}=O units having an additional carboxylate bridge to reconcile the unusually short Fe−Fe bond distance compared with synthetic model complexes with $\{Fe_2O_2\}^{n+}$ core structures (Table 2). The inability of the sole di(μ-oxo)diiron(IV) model complex[40] and various high-level density functional theory (DFT) calculations[14,15] to reproduce the short Fe−Fe bond distance underscores the need for additional structural characterization of this intermediate.

The reactivity patterns of several model complexes also suggest reconsideration of the proposed structure of Q. Reaction of $[Fe_2(H_2Hbamb)_2(N\text{-}meIm)_2]$, where H_4HBamb is 2,3-bis(2-hydroxybenzamido)-dimethylbutane and meIm is *N*-methylimizadole, with oxygen atom donors resulted in formation of a diiron(II/IV) complex having a terminal FeIV=O unit capable of oxidizing cyclohexane to cyclohexanol.[41] In this example, the potency of the system was achieved by concentrating the oxidizing capability at the Fe(IV) center. The authors proposed that an analogous diiron(III/V) center (**10**) might be responsible for methane oxidation in MMOH. A separate investigation found that the valence-localized $[OH—Fe^{III}—O—Fe^{IV}=O]^{2+}$ form of a synthetic complex supported by tris((4-methoxy-3,5-dimethylpyridin-2-yl)methyl)amine cleaves strong C−H bonds a million-fold more rapidly than its valence-delocalized $[Fe^{3.5}(\mu\text{-}O)_2Fe^{3.5}]^{3+}$ "diamond core" analogue.[42] A third study revealed the rate of 9,10-dihydroanthrocene oxidation by $[Fe^{IV}{}_2(\mu\text{-}O)_2L_2]^{4+}$, where L = tris((4-methoxy-3,5-dimethylpyrid-2-yl)d_2-methyl)amine, to be significantly slower for than that by $[Fe^{IV}(O)(L)(NCMe)]^{2+}$, the corresponding mononuclear Fe^{IV}=O complex of the same ligand.[40] Together, these data suggest that an oxidant with a terminal Fe=O unit (**11** or **12**) might be more effective for C−H bond cleavage than one having an oxo-bridged Fe−O−Fe center and indicate that further structural characterization of Q is necessary to understand better how this intermediate hydroxylates methane. RFQ coupled with advanced spectroscopic methods, such as cryoreduction/ENDOR, resonance Raman, and possibly nuclear resonance vibrational spectroscopy, can aid in characterizing Q. To date, application of these methods to the intermediates of MMO has proved difficult, however. Advances in spectroscopic methodology and possibly sample preparation may help to overcome past failures.

One point regarding the structure of Q that requires further consideration is whether the RFQ-trapped intermediate studied by EXAFS spectroscopy is the same species identified in stopped-flow kinetic studies.[41] To activate the strong C−H bond of methane, Q must be an extremely potent oxidant; however, its oxidizing power must be controlled to prevent oxidative damage to the protein. Given

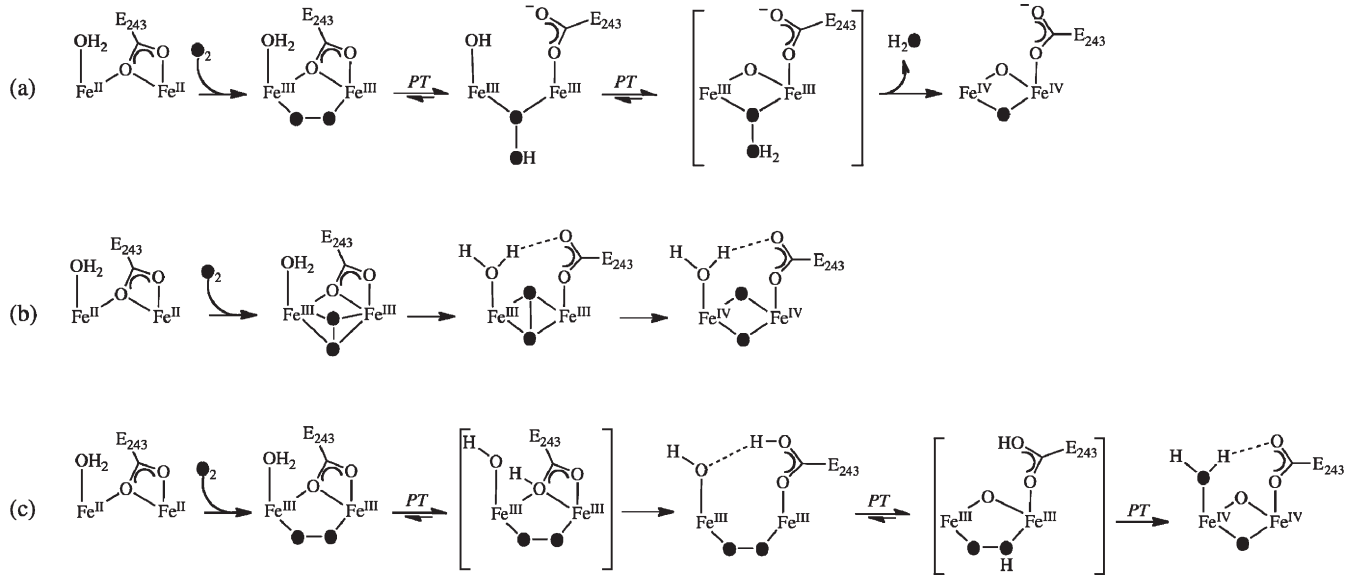

FIGURE 6. Three proposed mechanisms for Q formation. (a) Proton-assisted heterolytic O−O bond cleavage involving a stable hydroperoxide intermediate. (b) Proton-independent homolytic O−O bond cleavage. (c) Proton-assisted heterolytic O−O bond cleavage involving protonation and rearrangement of E243 prior to Q formation.

recent biomimetic findings (vide supra), it is not unlikely that Q collapses to a more thermodynamically stable species, such as a "diamond core", to protect the enzyme from self-destruction in the absence of substrate. It is therefore necessary to prove that RFQ-trapped samples of Q are chemically competent.

Q reacts rapidly with methane and other substrates.[10,21,23,43] Mechanistic considerations are reviewed elsewhere.[44] In the absence of substrate, Q decays by acquiring two electrons and two protons to regenerate $MMOH_{ox}$. The mechanism of this transformation is largely unknown, but recent kinetic studies of *Mc* MMOH have identified a species, Q*, that lies on this pathway.[24] Q* displays a unique shoulder at 455 nm in its optical spectrum and has a decay rate constant unaffected by CH_4. Additional spectroscopic properties of this species have not been determined.

The Role of Protons during O_2 Activation

The role of protons during sMMO O_2 activation has been a controversial topic. Early studies of cytochrome P450s, heme monooxygenases that activate strong C−H bonds in a fashion similar to sMMO, revealed that sequential transfer of two protons to the distal oxygen atom of a dioxygen unit bound terminally to the iron center provides the driving force for heterolytic O−O bond cleavage. This event results in the release of a water molecule and formation of the iron(IV)−ligand radical species responsible for the hydroxylation chemistry.[45] Based on these findings, a similar type of mechanism was envisioned for sMMO (Figure 6a).

The first studies probing proton involvement in sMMO, performed by our group, concluded that proton transfer is not rate-determining for any of the O_2 activation events, including O−O bond cleavage.[11] We employed stopped-flow optical spectroscopy to probe the proton dependences of the events that occur upon rapidly mixing a solution of *Mc* $MMOH_{red}$ and MMOB prepared in 10 mM MOPS at pH 7.0 with O_2-saturated 100 mM buffer having the desired reaction pH.[11] When this method was used, all of the O_2 activation processes monitored were independent of pH between pH 6.6 and 8.6 at 4 °C. An examination of the same reaction in D_2O showed a negligible effect of isotopic substitution.[11,46] Together these two observations suggested that proton transfer is not rate-determining for any of the processes monitored. We proposed a mechanism involving proton-independent, homolytic O−O bond cleavage (Figure 6b), although the studies did not rule out the possibility that fast proton transfer (i.e., not rate-determining) did occur during the steps investigated.

Subsequent, contrasting findings were reported for *Mt* MMOH.[47] The authors of these studies also utilized stopped-flow optical spectroscopy to investigate the effects of pH and D_2O on events resulting from the reaction of $MMOH_{red}$ and MMOB with O_2-saturated buffer. For pH dependence experiments, protein samples were preincubated at the desired reaction pH. The experiments revealed that H_{peroxo} formation and H_{peroxo} to Q conversion, but not Q decay, were pH-dependent between pH 6.5 and 8.6 at 4 °C. Both

SCHEME 1. Proposed Models Describing the Role of Protons during MMOH O_2 Activation

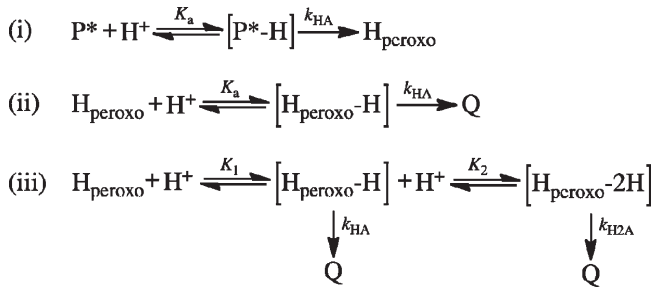

pH-dependent processes displayed sigmoidal pH rate profiles revealing negligible activity at high pH. That for H_{peroxo} formation was fit to the mathematical description of Scheme 1, model i, describing a single, reversible ionization of P* followed by irreversible conversion to H_{peroxo}. A pK_a value of 7.6 was assigned from the data fit. Similarly, the pH rate profile of H_{peroxo} to Q conversion was fit to the equation describing Scheme 1, model ii, with a pK_a of 7.6.

A second piece of evidence that protons played an important role during O_2 activation was the observation that experiments performed in D_2O returned kinetic solvent isotope effects (KSIEs) of $k_H/k_D = 1.3 \pm 0.1$ for H_{peroxo} formation and 1.4 ± 0.1 for H_{peroxo} to Q conversion. Proton inventory plots constructed by measuring the rate constants in varying mole fractions of D_2O were linear for both processes, suggesting that a single proton is transferred in the transition state for each step. This observation was interpreted as evidence that the proton transfer reactions occur at the active site and do not result from protein-based conformational or complexation changes, because the latter are likely to involve multiple proton transfers. Building from analogy to the cytochrome P450 monooxygenases and observing that the measured pK_a values and proton inventory fractionation factors were consistent with a coordinated water molecule, the authors suggested the mechanism of Figure 6a.

We recently reexamined O_2 activation in the *Mc* system.[24] Experiments were performed by rapidly mixing a solution of $MMOH_{red}$ and MMOB preequilibrated at the appropriate pH with O_2-saturated buffer. The data showed conclusively that proton transfer is rate-determining for P* to H_{peroxo} and H_{peroxo} to Q conversion but not for P* formation, Q to Q* conversion, or Q* decay at 4 °C. As in the *Mt* system, the pH rate profile of P* to H_{peroxo} conversion fit well to the analytical equation describing Scheme 1, model i, with a pK_a value of 7.2. Unlike the *Mt* system, however, the pH rate profile of H_{peroxo} to Q conversion did not fit well to the mathematical solution of Scheme 1, model ii. Instead, model iii, describing a doubly ionizing system, was necessary to fit the data. pK_a values extracted from the fits were p$K_1 = 7.9$ and p$K_2 = 7.0$. A likely explanation for the differences observed in the two *Mc* experiments is the procedure employed. The early experiments relied on a pH jump instead of a preincubation. The former depends on the ability of the active site to equilibrate with the bulk solvent on the experimental time scale. Probably such was not the case, because the hydrophobic nature of the MMOH active site cavity will make it difficult for the external pH to be realized at the site of the reaction chemistry for the faster time scale of the pH jump experiment.

We also reexamined the KSIEs for the *Mc* O_2 activation events.[24] Experiments performed in D_2O returned values of 2.0 ± 0.2 for P* to H_{peroxo} conversion and 1.8 ± 0.3 for H_{peroxo} to Q conversion, further supporting a role for proton transfer during these steps. On the basis of these data, we proposed a mechanism in which proton transfer promotes O−O bond cleavage (Figure 6c). Because it is likely that E243 must dissociate from its bridging position to allow for Q formation, the recent finding that treatment of $[Fe_2(\mu\text{-}O_2)(N\text{-EtHPTB})(\mu\text{-}PhCO_2)]^{2+}$ and $[Fe_2(\mu\text{-}O_2)(N\text{-EtHPTB})(\mu\text{-}C_6F_5CO_2)]^{2+}$, where HPTB is *N*,*N*,*N*′,*N*′-tetrakis(2-benzimidazolylmethyl)-2-hydroxy-1,3-diaminopropane, with acid leads to protonation and dissociation of the bridging carboxylate instead of the peroxide moiety,[48] and a theoretical study showing that protonation of the RNR-R2 peroxodiiron(III) unit does not result in a stable hydroperoxide,[49] we proposed that the first proton is transferred to E243 instead of the peroxide unit. Additional support for this mechanism comes from the similarity between the spectroscopic properties of P* and H_{peroxo}, suggesting that their iron−oxygen cores are the same. The spectroscopic properties of peroxodiiron(III) and hydroperoxodiiron(III) units are expected to be different, however.[49]

The Future of sMMO

Although sMMO has been a topic of intense biochemical investigation for over 30 years, many aspects of its important chemistry remain enigmatic. As with any longstanding scientific problem, the questions that remain about the system are difficult ones to answer. What are the structures of P*, H_{peroxo}, and Q? What makes Q such a potent oxidant and can we use that information to design new catalysts? Is it possible to engineer the system at a protein or whole-cell scale suitable for industrial production of alternative fuels and for bioremediation purposes? Given the current environmental challenges that face our society, we believe that it

is crucial to continue to investigate how this catalyst works. With new findings and advances in spectroscopic tools, the coming years should bring to light a new era in sMMO chemistry.

The structure of intermediate Q and to a lesser extent those of H_{peroxo} and P* remain top priorities in the field. Another challenge that has hampered our understanding of this enzyme is the inability to generate sufficient quantities of soluble enzyme bearing site-directed amino acid substitutions in a robust manner. Breakthroughs in the bioengineering of the system for additional biochemical and spectroscopic studies will require more fundamental knowledge of the protein factors involved in its copper-dependent transcriptional and translational regulation. An additional question central to the study of diiron proteins is what properties of MMOH cause H_{peroxo} to spontaneously convert to Q whereas the peroxodiiron(III) units of most other diiron enzymes do not appear to access such high-valent intermediates. By addressing these questions as a community, we hope to gain new insights into this important system.

Work from our laboratory discussed in this Account was funded by Grant GM032134 from the National Institute of General Medical Sciences.

BIOGRAPHICAL INFORMATION

Professor Stephen J. Lippard is the Arthur Amos Noyes Professor of Chemistry at the Massachusetts Institute of Technology. His research areas lie at the interface of inorganic chemistry and biology.

Dr. Christine E. Tinberg received her Bachelor of Arts in chemistry from Northwestern University in 2005, where she performed research in the laboratory of Amy Rosenzweig. In 2010, Christine received her doctorate in biochemistry at the Massachusetts Institute of Technology under Prof. Lippard, investigating the reactivity of bacterial multicomponent monooxygenases.

FOOTNOTES

*To whom correspondence should be addressed. E-mail: lippard@mit.edu. Telephone: (617) 253-1892. Fax: (617) 258-8150.

REFERENCES

1 Arakawa, H.; Aresta, M.; Armor, J. N.; Barteau, M. A.; Beckman, E. J.; Bell, A. T.; Bercaw, J. E.; Creutz, C.; Dinjus, E.; Dixon, D. A.; Domen, K.; DuBois, D. L.; Eckert, J.; Fujita, E.; Gibson, D. H.; Goddard, W. A.; Goodman, D. W.; Keller, J.; Kubas, G. J.; Kung, H. H.; Lyons, J. E.; Manzer, L. E.; Marks, T. J.; Morokuma, K.; Nicholas, K. M.; Periana, R.; Que, L.; Rostrup-Nielson, J.; Sachtler, W. M. H.; Schmidt, L. D.; Sen, A.; Somorjai, G. A.; Stair, P. C.; Stults, B. R.; Tumas, W. Catalysis Research of Relevance to Carbon Management: Progress, Challenges, and Opportunities. *Chem. Rev.* **2001**, *101*, 953–996.

2 Balasubramanian, R.; Smith, S. M.; Rawat, S.; Yatsunyk, L. A.; Stemmler, T. L.; Rosenzweig, A. C. Oxidation of Methane by a Biological Dicopper Centre. *Nature* **2010**, *465*, 115–119.

3 Merkx, M.; Kopp, D. A.; Sazinsky, M. H.; Blazyk, J. L.; Müller, J.; Lippard, S. J. Dioxygen Activation and Methane Hydroxylation by Soluble Methane Monooxygenase: A Tale of Two Irons and Three Proteins. *Angew. Chem., Int. Ed.* **2001**, *40*, 2782–2807.

4 Wallar, B. J.; Lipscomb, J. D. Dioxygen Activation by Enzymes Containing Binuclear Non-Heme Iron Clusters. *Chem. Rev.* **1996**, *96*, 2625–2657.

5 Friedle, S.; Reisner, E.; Lippard, S. J. Current Challenges of Modeling Diiron Enzyme Active Sites for Dioxygen Activation by Biomimetic Synthetic Complexes. *Chem. Soc. Rev.* **2010**, *39*, 2768–2779.

6 Rosenzweig, A. C.; Frederick, C. A.; Lippard, S. J.; Nordlund, P. Crystal Structure of a Bacterial Non-Haem Iron Hydroxylase That Catalyses the Biological Oxidation of Methane. *Nature* **1993**, *366*, 537–543.

7 Whittington, D. A.; Lippard, S. J. Crystal Structures of the Soluble Methane Monooxygenase Hydroxylase from *Methylococcus capsulatus* (Bath) Demonstrating Geometrical Variability at the Dinuclear Iron Active Site. *J. Am. Chem. Soc.* **2001**, *123*, 827–838.

8 Whittington, D. A.; Rosenzweig, A. C.; Frederick, C. A.; Lippard, S. J. Xenon and Halogenated Alkanes Track Putative Substrate Binding Cavities in the Soluble Methane Monooxygenase Hydroxylase. *Biochemistry* **2001**, *40*, 3476–3482.

9 Murray, L. J.; Lippard, S. J. Substrate Trafficking and Dioxygen Activation in Bacterial Multicomponent Monooxygenases. *Acc. Chem. Res.* **2007**, *40*, 466–474.

10 Lee, S.-K.; Nesheim, J. C.; Lipscomb, J. D. Transient Intermediates of the Methane Monooxygenase Catalytic Cycle. *J. Biol. Chem.* **1993**, *268*, 21569–21577.

11 Liu, K. E.; Valentine, A. M.; Wang, D.; Huynh, B. H.; Edmondson, D. E.; Salifoglou, A.; Lippard, S. J. Kinetic and Spectroscopic Characterization of Intermediates and Component Interactions in Reactions of Methane Monooxygenase from *Methylococcus capsulatus* (Bath). *J. Am. Chem. Soc.* **1995**, *117*, 10174–10185.

12 Stahl, S. S.; Francisco, W. A.; Merkx, M.; Klinman, J. P.; Lippard, S. J. Oxygen Kinetic Isotope Effects in Soluble Methane Monooxygenase. *J. Biol. Chem.* **2001**, *276*, 4549–4553.

13 Bollinger, J. M., Jr.; Krebs, C. Stalking Intermediates in Oxygen Activation by Iron Enzymes: Motivation and Method. *J. Inorg. Biochem.* **2006**, *100*, 586–605.

14 Gherman, B. F.; Baik, M.-H.; Lippard, S. J.; Friesner, R. A. Dioxygen Activation in Methane Monooxygenase: A Theoretical Study. *J. Am. Chem. Soc.* **2004**, *126*, 2978–2990.

15 Rinaldo, D.; Philipp, D. M.; Lippard, S. J.; Friesner, R. A. Intermediates in Dioxygen Activation by Methane Monooxygenase: A QM/MM Study. *J. Am. Chem. Soc.* **2007**, *129*, 3135–3147.

16 *Myo*-inositol oxygenase, which activates O_2 at a mixed-valent diiron(II/III) center, utilizes a superoxodiiron(III) unit to oxidize *myo*-inositol. Xing, G.; Diao, Y.; Hoffart, L. M.; Barr, E. W.; Prabhu, K. S.; Arner, R. J.; Reddy, C. C.; Krebs, C.; Bollinger, J. M., Jr. Evidence for C−H Cleavage by an Iron-Superoxide Complex in the Glycol Cleavage Reaction Catalyzed by *myo*-Inositol Oxygenase. *Proc. Natl. Acad. Sci. U.S.A.* **2006**, *103*, 6130–6135.

17 Synthetic mixed-valent diiron(II/III) complexes can oxidize external substrates. Shan, X.; Que, L., Jr. Intermediates in the Oxygenation of a Nonheme Diiron(II) Complex, Including the First Evidence for a Bound Superoxo Species. *Proc. Natl. Acad. Sci. U.S.A.* **2005**, *102*, 5340–5345. Zhao, M.; Helms, B.; Slonkina, E.; Friedle, S.; Lee, D.; DuBois, J.; Hedman, B.; Hodgson, K. O.; Fréchet, J. M. J.; Lippard, S. J. Iron Complexes of Dendrimer-Appended Carboxylates for Activating Dioxygen and Oxidizing Hydrocarbons. *J. Am. Chem. Soc.* **2008**, *130*, 4352–4363.

18 Liu, K. E.; Wang, D.; Huynh, B. H.; Edmondson, D. E.; Salifoglou, A.; Lippard, S. J. Spectroscopic Detection of Intermediates in the Reaction of Dioxygen with the Reduced Methane Monooxygenase Hydroxylase from *Methylococcus capsulatus* (Bath). *J. Am. Chem. Soc.* **1994**, *116*, 7465–7466.

19 H_{peroxo} is denoted L in early studies of *Mc* MMOH and P in studies of *Mt* MMOH.

20 Shu, L.; Nesheim, J. C.; Kauffmann, K.; Münck, E.; Lipscomb, J. D.; Que, L., Jr. An $Fe_2^{IV}O_2$ Diamond Core Structure for the Key Intermediate Q of Methane Monooxygenase. *Science* **1997**, *275*, 515–518.

21 Valentine, A. M.; Stahl, S. S.; Lippard, S. J. Mechanistic Studies of the Reaction of Reduced Methane Monooxygenase Hydroxylase with Dioxygen and Substrates. *J. Am. Chem. Soc.* **1999**, *121*, 3876–3887.

22 We recently remeasured this value to be 0.75 s^{-1}.

23 Brazeau, B. J.; Lipscomb, J. D. Kinetics and Activation Thermodynamics of Methane Monooxygenase Compound Q Formation and Reaction with Substrates. *Biochemistry* **2000**, *39*, 13503–13515.

24 Tinberg, C. E.; Lippard, S. J. Revisiting the Mechanism of Dioxygen Activation in Soluble Methane Monooxygenase from *M. capsulatus* (Bath): Evidence for a Multi-Step, Proton-Dependent Reaction Pathway. *Biochemistry* **2009**, *48*, 12145–12158.

25 Moënne-Loccoz, P.; Baldwin, J.; Ley, B. A.; Loehr, T. M.; Bollinger, J. M., Jr. O_2 Activation by Non-Heme Diiron Proteins: Identification of a Symmetric μ-1,2-Peroxide in a Mutant of Ribonucleotide Reductase. *Biochemistry* **1998**, *37*, 14659–14663.

26 Skulan, A. J.; Brunold, T. C.; Baldwin, J.; Saleh, L.; Bollinger, J. M., Jr.; Solomon, E. I. Nature of the Peroxo Intermediate of the W48F/D84E Ribonucleotide Reductase Variant: Implications for O_2 Activation by Binuclear Non-Heme Iron Enzymes. *J. Am. Chem. Soc.* **2004**, *126*, 8842–8855.

27 Moënne-Loccoz, P.; Krebs, C.; Herlihy, K.; Edmondson, D. E.; Theil, E. C.; Huynh, B. H.; Loehr, T. M. The Ferroxidase Reaction of Ferritin Reveals a Diferric μ-1,2 Bridging Peroxide Intermediate in Common with Other O_2-Activating Non-Heme Diiron Proteins. *Biochemistry* **1999**, *38*, 5290–5295.

28 Broadwater, J. A.; Ai, J.; Loehr, T. M.; Sanders-Loehr, J.; Fox, B. G. Peroxodiferric Intermediate of Stearoyl-Acyl Carrier Protein Δ^9 Desaturase: Oxidase Reactivity during Single Turnover and Implications for the Mechanism of Desaturation. *Biochemistry* **1998**, *37*, 14664–14671.

29 Vu, V. V.; Emerson, J. P.; Martinho, M.; Kim, Y. S.; Münck, E.; Park, M. H.; Que, L., Jr. Human Deoxyhypusine Hydroxylase, an Enzyme Involved in Regulating Cell Growth, Activates O_2 with a Nonheme Diiron Center. *Proc. Natl. Acad. Sci. U.S.A.* **2009**, *106*, 14814–14819.

30 Bailey, L. J.; Fox, B. G. Crystallographic and Catalytic Studies of the Peroxide-Shunt Reaction in a Diiron Hydroxylase. *Biochemistry* **2009**, *48*, 8932–8939.

31 These conclusions were based on modeling the active site $2F_o - F_c$ difference density as H_2O_2 by employing an O−O bond distance restraint of 1.5 Å; using this approach, the Fe−O bond distances are too long to assign the unit as a peroxodiiron(III) species. Attempts to release the restraint and refine the structure resulted in an increased O−O bond distance of 1.8 Å and decreased Fe−O bond distances of ∼2.1 Å, neither of which support the peroxide formulation.

32 Tshuva, E. Y.; Lippard, S. J. Synthetic Models for Non-Heme Carboxylate-Bridged Diiron Metalloproteins: Strategies and Tactics. *Chem. Rev.* **2004**, *104*, 987–1012.

33 Kim, K.; Lippard, S. J. Structure and Mössbauer Spectrum of a (μ-1,2-Peroxo)bis(μ-carboxylato)diiron(III) Model for the Peroxo Intermediate in the Methane Monooxygenase Hydroxylase Reaction Cycle. *J. Am. Chem. Soc.* **1996**, *118*, 4914–4915.

34 Han, W.-G.; Noodleman, L. Structural Model Studies for the Peroxo Intermediate P and the Reaction Pathway from P → Q of Methane Monooxygenase Using Broken-Symmetry Density Functional Calculations. *Inorg. Chem.* **2008**, *47*, 2975–2986.

35 Siegbahn, P. E. M. O—O Bond Cleavage and Alkane Hydroxylation in Methane Monooxygenase. *J. Biol. Inorg. Chem.* **2001**, *6*, 27–45.

36 Bochevarov, A. D.; Li, J.; Song, W. J.; Friesner, R. A.; Lippard, S. J. Insights Into the Different Dioxygen Activation Pathways of Methane and Toluene Monooxygenase Hydroxylases. 2010, Manuscript in Preparation.

37 Beauvais, L. G.; Lippard, S. J. Reactions of the Peroxo Intermediate of Soluble Methane Monooxygenase Hydroxylase with Ethers. *J. Am. Chem. Soc.* **2005**, *127*, 7370–7378.

38 Tinberg, C. E.; Lippard, S. J. Oxidation Reactions Performed by Soluble Methane Monooxygenase Hydroxylase Intermediates H_{peroxo} and Q Proceed by Distinct Mechanisms. *Biochemistry* **2010**, *49*, 7902–7912.

39 Lee, S.-K.; Fox, B. G.; Froland, W. A.; Lipscomb, J. D.; Münck, E. A Transient Intermediate of the Methane Monooxygenase Catalytic Cycle Containing an $Fe^{IV}Fe^{IV}$ Cluster. *J. Am. Chem. Soc.* **1993**, *115*, 6450–6451.

40 Xue, G.; Wang, D.; De Hont, R.; Fiedler, A. T.; Shan, X.; Münck, E.; Que, L., Jr. A Synthetic Precedent for the $[Fe^{IV}_2(\mu\text{-}O)_2]$ Diamond Core Proposed for Methane Monooxygenase Intermediate Q. *Proc. Natl. Acad. Sci. U.S.A.* **2007**, *104*, 20713–20718.

41 Rowe, G. T.; Rybak-Akimova, E. V.; Caradonna, J. P. Unraveling the Reactive Species of a Functional Non-Heme Iron Monooxygenase Model Using Stopped-Flow UV-Vis Spectroscopy. *Inorg. Chem.* **2007**, *46*, 10594–10606.

42 Xue, G.; De Hont, R.; Münck, E.; Que, L., Jr. Million-Fold Activation of the $[Fe_2(\mu\text{-}O)_2]$ Diamond Core for C—H Bond Cleavage. *Nat. Chem.* **2010**, *2*, 400–405.

43 Ambundo, E. A.; Friesner, R. A.; Lippard, S. J. Reactions of Methane Monooxygenase Intermediate Q with Derivatized Methanes. *J. Am. Chem. Soc.* **2002**, *124*, 8770–8771.

44 Baik, M.-H.; Newcomb, M.; Friesner, R. A.; Lippard, S. J. Mechanistic Studies on the Hydroxylation of Methane by Methane Monooxygenase. *Chem. Rev.* **2003**, *103*, 2385–2419.

45 Denisov, I. G.; Makris, T. M.; Sligar, S. G.; Schlichting, I. Structure and Chemistry of Cytochrome P450. *Chem. Rev.* **2005**, *105*, 2253–2277.

46 The pD values of the buffers employed in these experiments were not corrected for deuterium istope effect.

47 Lee, S.-K.; Lipscomb, J. D. Oxygen Activation Catalyzed by Methane Monooxygenase Hydroxylase Component: Proton Delivery during the O—O Bond Cleavage Steps. *Biochemistry* **1999**, *38*, 4423–4432.

48 Do, L. H.; Hayashi, T.; Moënne-Loccoz, P.; Lippard, S. J. Carboxylate as the Protonation Site in (Peroxo)diiron(III) Model Complexes of Soluble Methane Monooxygenase and Related Diiron Proteins. *J. Am. Chem. Soc.* **2010**, *132*, 1273–1275.

49 Jensen, K. P.; Bell, C. B., III; Clay, M. D.; Solomon, E. I. Peroxo-Type Intermediates in Class 1 Ribonucleotide Reductase and Related Binuclear Non-Heme Iron Enzymes. *J. Am. Chem. Soc.* **2009**, *131*, 12155–12171.

50 Bollinger, J. M., Jr.; Krebs, C.; Vicol, A.; Chen, S.; Ley, B. A.; Edmondson, D. E.; Huynh, B. H. Engineering the Diiron Site of *Escherichia coli* Ribonucleotide Reductase Protein R2 to Accumulate an Intermediate Similar to H_{peroxo}, the Putative Peroxodiiron(III) Complex from the Methane Monooxygenase Catalytic Cycle. *J. Am. Chem. Soc.* **1998**, *120*, 1094–1095.

51 Broadwater, J. A.; Achim, C.; Münck, E.; Fox, B. G. Mössbauer Studies of the Formation and Reactivity of a Quasi-Stable Peroxo Intermediate of Stearoyl-Acyl Carrier Protein Δ^9-Desaturase. *Biochemistry* **1999**, *38*, 12197–12204.

52 Pereira, A. S.; Small, W.; Krebs, C.; Tavares, P.; Edmondson, D. E.; Theil, E. C.; Huynh, B. H. Direct Spectroscopic and Kinetic Evidence for the Involvement of a Peroxodiferric Intermediate during the Ferroxidase Reaction in Fast Ferritin Mineralization. *Biochemistry* **1998**, *37*, 9871–9876.

53 Zhang, X.; Furutachi, H.; Fujinami, S.; Nagatomo, S.; Maeda, Y.; Watanabe, Y.; Kitagawa, T.; Suzuki, M. Structural and Spectroscopic Characterization of (μ-Hydroxo or μ-Oxo)(μ-peroxo)diiron(III) Complexes: Models for Peroxo Intermediates of Non-Heme Diiron Proteins. *J. Am. Chem. Soc.* **2005**, *127*, 826–827.

54 Dong, Y.; Zang, Y.; Shu, L.; Wilkinson, E. C.; Que, L., Jr.; Kauffmann, K.; Münck, E. Models for Nonheme Diiron Enzymes. Assembly of a High-Valent $Fe_2(\mu\text{-}O)_2$ Diamond Core from Its Peroxo Precursor. *J. Am. Chem. Soc.* **1997**, *119*, 12683–12684.

55 Dong, Y.; Fujii, H.; Hendrich, M. P.; Leising, R. A.; Pan, G.; Randall, C. R.; Wilkinson, E. C.; Zang, Y.; Que, L., Jr.; Fox, B. G.; Kauffmann, K.; Münck, E. A High-Valent Nonheme Iron Intermediate. Structure and Properties of $[Fe_2(\mu\text{-}O)_2(5\text{-Me-TPA})_2](ClO_4)_3$. *J. Am. Chem. Soc.* **1995**, *117*, 2778–2792.

56 Dong, Y.; Que, L., Jr.; Kauffmann, K.; Münck, E. An Exchange-Coupled Complex with Localized High-Spin Fe^{IV} and Fe^{III} Sites of Relevance to Cluster X of *Escherichia coli* Ribonucleotide Reductase. *J. Am. Chem. Soc.* **1995**, *117*, 11377–11378.

57 Hsu, H.-F.; Dong, Y.; Shu, L.; Young, V. G., Jr.; Que, L., Jr. Crystal Structure of a Synthetic High-Valent Complex with an $Fe_2(\mu\text{-}O)_2$ Diamond Core. Implications for the Core Structures of Methane Monooxygenase Intermediate Q and Ribonucleotide Reductase Intermediate X. *J. Am. Chem. Soc.* **1999**, *121*, 5230–5237.